

# Reconstructing 3D Motion Trajectory of Large Swarm of Flying Objects

Danping Zou and Yan Qiu Chen

**Abstract**—This paper addresses the problem of reconstructing the motion trajectories of the individuals in a large collection of flying objects using two temporally synchronized and geometrically calibrated cameras. The 3D trajectory reconstruction problem involves two challenging tasks - stereo matching and temporal tracking. Existing methods separate the two and process them one at a time sequentially, and suffer from frequent irresolvable ambiguities in stereo matching and in tracking. We unify the two tasks, and propose an optimization approach to solving stereo matching and temporal tracking simultaneously. It treats 3D trajectory acquisition problem as selecting appropriate stereo correspondence out of all possible ones for each object via minimizing a cost function. Experiment results show that the proposed method offers significant performance advantage over existing approaches. The proposed method has successfully been applied to reconstruct 3D motion trajectories of hundreds of simultaneously flying fruit flies (*Drosophila Melanogaster*), which could facilitate the study the insect's collective behavior.

**Index Terms**—Multiple object 3D tracking, 3D motion trajectories, Swarms, Collective behavior, Fruit flies.

## 1 INTRODUCTION

A PREVALENT phenomenon in nature is aggregations of objects moving in a 3D space, such as insect swarms, bird flocks, and fish schools. These subjects tend to create complex dynamic behavior. Birds and fish gather in vast numbers, keeping some sort of cohesion in movement and creating fascinating patterns [1] [2]. Migrating butterflies fly within a bounded layer above the ground towards one direction [3]. Bats simultaneously emerge in great number from cave and soar in the sky at dusk [4]. Studying the collective behavior of these animal aggregations is of great value to a wide range of fields, including evolutionary biology, artificial intelligence [5], computer graphics [6], control theory [7], engineering [8], economics [9] and social sciences [10].

An effective way to study the behavior of animal aggregations is through accurately measuring the 3D motion pattern of these subjects, or in other words, measuring how the 3D location of each individual varies with time. Quantitative analysis can then be done to aid in discovering and explaining the underlying behavior patterns of the subjects. Since there had to date not been effective methods to measure the trajectory of each individual in a large swarm, visual inspection, instead of quantitative analysis, is used to make conjectures. Although some mathematical models such as [6] [11] [12], have successfully simulated the life-like collective behavior by assuming some simple rules, without accurate measurement data of real-world cases, as stated in [13], it cannot be verified that the living systems actually follow these rules. So the lack of effective methods

to measure the 3D motion trajectories of flying object aggregations has become a bottleneck of the current research on animal collective behavior.

A feasible way to measure the 3D motion trajectories of object aggregations is through using multiple cameras. It has several advantages over the sensor-based method in which some positioning and wireless communication devices are mounted on the subjects [14]. The vision-based method is able to accurately measure a large number of objects at a low cost and does not affect the behavior of the subjects.

The vision-based method to recover the time-varying 3D coordinates of the objects involves two tasks, namely, stereo matching - establishing stereo correspondences across views, and tracking - finding motion correspondences for each object. In the case of a large number of visually identical objects flying in a 3D space, both tasks are challenging since no appearance cue (such as color, texture, and shape) is available to distinguish the individuals. There has been research on the problem but no satisfactory solution has been published.

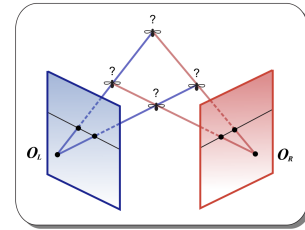


Fig. 1. The object on the left image has multiple matching candidates on the right image satisfying the epipolar constraint resulting in stereo matching ambiguity.

• School of Computer Science, Fudan University, Shanghai, China.  
E-mail: [dpzou/chenyq]@fudan.edu.cn

Preliminary results of the research work described in this paper were presented at ICCV 2009. This draft was finished at Oct, 2011.

Existing related approaches are generally found in the applications of multi-camera tracking, such as tracking

pedestrians or feature points in multiple cameras, which can be classified into two major groups. The first category of methods establish stereo correspondences first frame by frame to reconstruct 3D locations of the objects. The 3D locations corresponding to the same object are then temporally associated to yield 3D trajectories [15]–[18]. This kind of methods work well when the number of objects is small or each object carries sufficient distinctive visual appearance that can be used to identify itself from the others. To deal with a large group of objects containing many visually identical objects, problems arise - multiple matching candidates are often present in stereo matching (see Fig. 1). It is impossible to identify which candidate is the genuine stereo correspondence, as the objects are visually indistinguishable. The stereo matching ambiguity happens so frequently that it makes the 3D coordinates reconstructed in the first step unreliable. Once the stereo matching ambiguity is incorrectly resolved, the final result will be greatly deteriorated by the incorrect 3D locations.

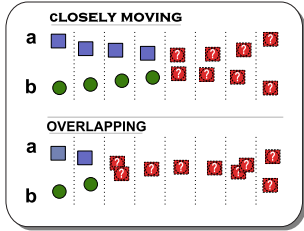


Fig. 2. Objects  $a$  and  $b$  overlap on the 2D image plane, leading to tracking ambiguity.

Approaches of the second category [19]–[21] track objects on each 2D image plane first. The resulting 2D tracks are then matched across views using inter-camera geometry and motion clues [19]. After that, 3D motion trajectories are reconstructed from the matched 2D tracks. The motivation behind this kind of methods is to utilize motions of objects on image planes to resolve single-frame matching ambiguity. This strategy is effective if the objects seldom overlap one another on image planes when the 2D motion trajectories of objects can be reliably acquired through tracking. For a dynamic particle swarm containing many objects flying in the 3D space, the images of these objects inevitably overlap at times. This poses a difficult situation for tracking (see Fig. 2), which likely causes failure in obtaining correct 2D tracks. Once 2D tracks are incorrect, matching the false tracks will result in severely corrupted 3D trajectories.

For the existing two types of methods, stereo matching and tracking are separated as two successive stages, where the first stage has a decisive influence on the final result. The difficulty is no matter which one is chosen as the first stage, such methods tend to produce poor performance for particle swarms. One naturally argues that stereo matching and tracking are in fact interwind in the problem of 3D trajectory reconstruction: stereo matching can be done much easier if tracking

results are known, while tracking on image planes can also be facilitated if stereo correspondences have been established at the current time step. A question arises : Is there a unified approach in which stereo matching and tracking are simultaneously performed to optimize the performance?

The answer is affirmative. We propose an optimization approach to reconstructing the 3D motion trajectories of flying object aggregations from two temporally synchronized and geometrically calibrated cameras, which unifies stereo matching and tracking into a whole. A key idea of this method is to treat each stereo pair of image objects as a *pairing* and convert the trajectory reconstruction problem into a process of selecting pairing sequence for each object. Through minimizing a cost function that incorporates cues from epipolar geometry, motion, and one-to-one match preference, the optimum pairing sequences of corresponding objects are obtained. The 3D motion trajectories are finally reconstructed by triangulation from the paired image locations. Both simulated and real-world experiments show remarkable performance of the proposed method. An illustrative example of the proposed method is given in Fig. 3.

The proposed method is able to deal with a large swarm of objects flying in the scene, and accommodate various kinetic models according to different situations. By adopting kinetic models on 2D image planes, the proposed method can also work in the case where the cameras are weakly calibrated - only the fundamental matrix between two cameras is known. The contribution of this paper is two fold:

- The paper presents a cost minimization method to solve the stereo matching and tracking in a unified manner, which according to our survey is the first effective method for reconstructing the 3D motion trajectories of flying particle-like objects from two calibrated and synchronized cameras
- To our best knowledge, this is the first time that the 3D motion trajectories of a swarm of hundreds of flying fruit flies are obtained, which could facilitate the study of the insect’s collective flight behavior.

The remainder of this paper will discuss related work in Section II. The 3D trajectory acquisition problem is formulated in Section III and a cost minimization approach is proposed in Section IV. Next, a sampling method based on solving assignment ranking problem is presented to optimize the objective function in Section V. Section VI discusses experimental results on both simulated and real-world swarms. The conclusion is drawn in Section VII.

## 2 RELATED WORK

### 2.1 Multi-object tracking techniques

Numerous approaches have been developed for tracking multiple objects, including Multiple Hypothesis Tracking(MHT) [22], Joint Probabilistic Data Association Filter(JPDF) [23], Greedy Assignment [24], and Particle

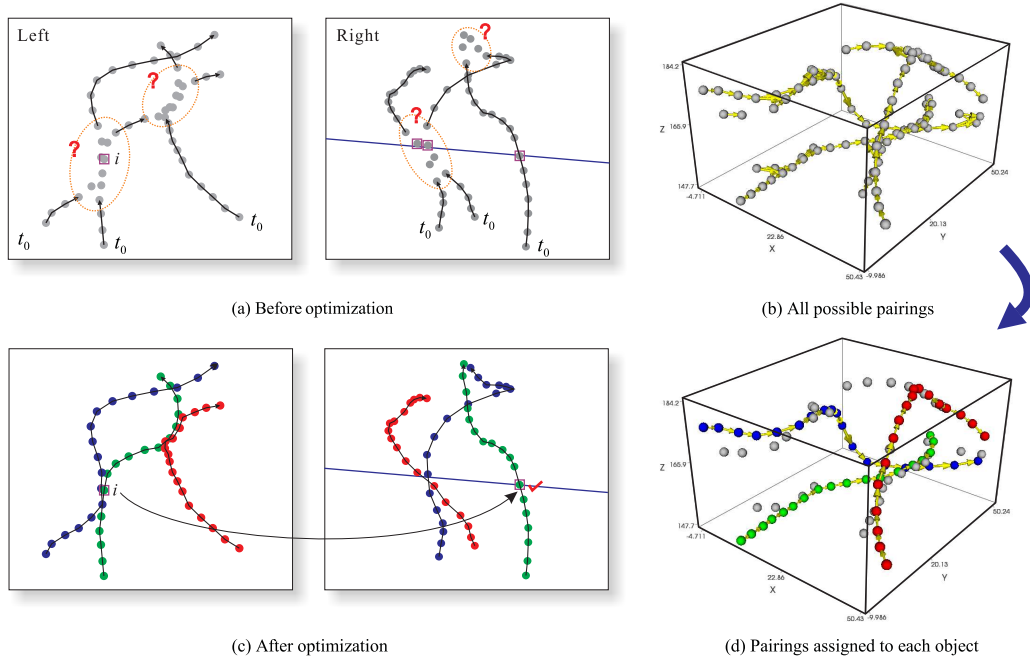


Fig. 3. An example illustrating the capability of the proposed method. In (a), tracking and stereo matching ambiguities both exist, e.g., the object  $i$  has multiple stereo matches in the right view and it also temporally corresponds to two possible positions at the next frame. After optimization, pairing sequences are obtained for each of the three objects (marked by red, green and blue) as shown in (d) and both ambiguities are resolved as shown in (c).

filter [25]. Two issues need to be addressed in multiple object tracking. The first one, known as data association, is to establish a mapping between measurements (e.g., image blobs) and objects at each time step. The second one is to estimate the motion states from the identified measurements for each object. For MHT [22], all feasible mappings between objects and measurements are enumerated and are thought of as a set of hypotheses. Probability of each hypothesis is propagated from prior hypothesis at previous time step. The associations are finally determined by selecting the best hypothesis with maximum probability over time. JPDAF [23] uses a similar way to evaluate the probability of each hypothesis, but instead of finding best hypothesis, it computes expectation of the motion state of objects over all hypotheses.

Both MHT and JPDAF use brute-force enumeration to generate legal hypotheses, leading to their incapability of coping with a large number of objects due to excessive computational complexity. To efficiently generate hypotheses, the authors of [26] [27] regard an association as a bipartite graph match, and then find the  $k$ -best hypotheses by recursively solving the assignment problem. Sometimes only the best hypothesis is obtained through one-step bipartite graph match, as the greedy optimal assignment (GOA) tracker [24] does. Although those bipartite-graph matching based algorithms significantly improve computational efficiency, their generated hypotheses are restrictive because they assume that a measurement can only be associated with no more than

one object and vice versa. This assumption does not always hold in practice, e.g., a measurement on image plane could correspond to several objects as a result of occlusion.

Another trend of methods is based on particle filter. The particle filter [25], approximating the probability density of motion state of an object conditioned on measurements by a set of weighted particles, is able to cope with tracking problem with non-linear measurement models and non-Gaussian noise where no analytic expression (closed formula) for probability density of motion state can be assumed. To solve the multi-object tracking problem, the particle-filter based methods collect all individual motion states into a single state variable and directly sample the probability densities of the joint motion state over time [28]. Unfortunately, the straightforward implementation of the joint particle filter by Sample Importance Resampling suffers from exponential complexity in the number of objects. Therefore, Markov Chain Monte Carlo (MCMC) technique is adopted to sample the high dimensional probability density of joint state [29]. Whereas, directly sampling in the continuous state space still requires extremely high computational cost and could fail in coping with a large number of objects. These existing multi-object tracking methods only focus on tracking objects on monocular video sequences. They are not capable of tracking the 3D positions of moving objects from stereo video sequences, since there is an additional issue in addition to tracking - stereo matching.

## 2.2 Reconstructing 3D motion trajectories of multiple objects

Most existing methods for recovering 3D motion trajectories of multiple objects apply techniques of multi-object tracking and stereo matching sequentially. The strategy of matching 2D tracks obtained through tracking on 2D image plane has been applied to reconstruct 3D trajectories of identical objects in binocular stereo [19]–[21]. The 2D tracks are however, not guaranteed to be correct, because objects on image planes may frequently overlap. Du et al. [19] suggested stop tracking at the time when interaction happens, and establish correspondence only for these partial 2D track segments. However, the common time span between segments could be too short to resolve stereo matching ambiguity. Although some stitching strategies can be applied, the resultant 3D trajectories can still be severely broken due to lengthy interactions as shown in Fig. 17.

A few methods incorporate tracking and stereo matching to generate more reliable results. Willneff et al. [30] proposed a spatial-temporal matching algorithm using motion prediction to reduce stereo matching ambiguities. Unfortunately, the algorithm would fail when stereo matching ambiguities become severe, since generating reliable prediction highly depends on correct 3D locations in the previous frame.

## 2.3 Animal and insect tracking for behavior research

Tracking animals using video sequences to facilitate the study of animal behavior, has increasingly attracted researchers in the computer vision and biology communities. Z. Khan et al. [31] tracked 2D trajectories of dozens of ants through MCMC-based particle filter. A. veeraraghavan et al. [32] track a bee dancing in a beehive by combining motion model and shape model to simultaneously obtain its 2D motion trajectory and shape changes. Authors in [33] obtained both trajectories and skeletons of flying birds through tracking on the image plane. In [34], a real-time system of tracking flying bats in a single view was developed. A single-camera system was presented in [35] to track and classify the behaviors of about 50 fruit flies moving on the 2D plane.

Biologists are not satisfied with acquiring only 2D motion trajectories for the study of subjects that fly or swim in 3D space. As early as in the 80's of the last century, researchers had attempted to obtain 3D trajectories of flying fruit flies [36], house flies [37], and bats [38] using two film cameras. In recent years, multiple digital video cameras are used to reconstruct 3D motion trajectories of fruit flies [18] [39]. But they can only deal with a few subjects by employing the existing techniques in computer vision. In [40], authors obtained the 3D positions of individuals in a starling flock by stereo matching, they however did not maintain their identities over time. The authors of [41] measured 3D motion trajectories of flying bats from three calibrated cameras by solving multiple-dimensional assignment problem based on the

epipolar constraint at a single video frame. But they presented 3D trajectories of only about ten flying bats in the video result. Recently, Straw et al. [42] proposed a real-time tracking system with eleven cameras to analyze the effects of visual contrast on the flight performance of fruit flies, but their system can only track a few insects.

## 3 PROBLEM STATEMENT

This paper studies the problem of reconstructing the 3D motion trajectory of each individual in a swarm of flying particle-like objects from multiple video sequences captured from different viewing directions. We focus on using two cameras due to its practical advantage of lower costs and easier deployment. It is not difficult to extend the proposed idea to the multiple camera case.

Suppose there are  $N$  objects flying in a 3D space. Two temporally synchronized and geometrically calibrated cameras capture the scene at time instances,  $t = 1, 2, \dots, T$ , producing two video sequences. The target blobs in the image can be detected and located by object detection techniques [43] [44]. We denote the detected blobs at time step  $t$  by a set  $M_t$ . The problem of trajectory reconstruction is to compute the time-varying 3D locations for each object from the observations - blobs detected from stereo video sequences,  $M_1, M_2, \dots, M_T$ .

## 4 METHOD

The trajectory reconstruction problem faces two challenges. One lies in the temporal domain, which is to establish motion correspondence between video frames. The other lies in the spatial domain, which is to find stereo correspondence across views. As discussed earlier (see Fig. 1 and Fig. 2), the two issues, if addressed separately, will cause ambiguities that are difficult to resolve. We propose a novel method in this paper that combines the two issues into a single problem and solve it by optimizing a unified objective function.

A key concept of the proposed method is 'pairing'. A pairing denotes a potential stereo correspondence, where the two paired image blobs may correspond to the same object. Denoting the blobs detected at respective views by  $M_t^{[1]}, M_t^{[2]}$ , the possible pairings at the time step  $t$  is given by  $M_t^{[1]} \times M_t^{[2]}$ . Each pairing is related to a 3D location by triangulating the centers of the two blobs. The trajectory reconstruction problem therefore becomes selecting the genuine pairings for each object over time.

In other words, the task is to select a sequence of pairings for each object. We name the pairings selected at each time step as a *configuration*, denoted by  $C_t = (c_t^1, \dots, c_t^n, \dots, c_t^N)$ . The problem we need to solve is to find out a sequence of configurations,  $C_{1:T} = (C_1, \dots, C_T)$  that best explain the target blobs recorded during the capturing process. To produce reasonable result, some knowledge is required to evaluate the quality of a given sequence of configurations. Define the evaluation function as  $f(\cdot)$ , which should incorporate all



aspects of knowledge about what a good configuration sequence should possess. Three cues are used. The first is epipolar constraint, which describes how a pairing geometrically fits as a correct stereo correspondence. The second is one-to-one match tendency. It is based on the observation that the majority of blobs have only one corresponding blob in the other view. The last is the knowledge about the motion of the objects. It describes how objects move and is used to ensure the reconstructed trajectories are consistent with the kinetic model of the objects. We will provide a detailed description about how these cues are mathematically formulated and incorporated into the evaluation function  $f(\cdot)$  in the following sections.

After that, the trajectory reconstruction problem becomes an optimization problem, that is, to find an optimum configuration sequence  $C_{1:T}^*$  that minimizes  $f(C_{1:T})$ :

$$C_{1:T}^* = \arg \min_{C_{1:T}} f(C_{1:T}). \quad (1)$$

When an optimum configuration sequence is obtained, the 3D motion trajectories can be computed by stereo triangulation for each pairing.

The number of objects present in the scene is usually a variable of the time, which makes the problem more challenging. In [31], a variable is introduced to indicate the set of visible objects at each time step, leading to a very complicated algorithm where the dimension of state space varies with iterations. Here, we use a dummy pairing  $\mathcal{O}$  to represent the absent state of objects. When objects have not shown up in the scene or have left the scene, they are simply assigned with  $\mathcal{O}$ . The advantage of this solution is that we can keep the dimension of the state space constant and do not have to resort to a complex algorithm that jumps among spaces of different dimensions. The drawback is the pairing sequences extracted from the same dimension of the configuration variable separated by the  $\mathcal{O}$  may not correspond to the same physical object. We can however treat these pairing sequences as belonging to different objects, since it is difficult to know whether an object that newly appears has shown up in the scene before.

The dimension of the configuration,  $N$ , can be determined by examining the maximum number of objects present in the scene throughout the time. The number of objects is usually estimated from the detected blobs in the video sequences. To account for the false detections and noises,  $N$  can be set slightly larger than the estimated number of objects.

#### 4.1 Epipolar constraint

If the blobs in different views correspond to the same 3D object, they will satisfy the epipolar constraint. This is an important cue for judging how likely a pair of blobs is a genuine stereo correspondence.

This implies that the blobs closer to epipolar lines of each other have higher likelihood of corresponding to

the same object. Denoting a non-dummy pairing by  $p$ , we define the cost of the pairing,  $p$ , being assigned to the object  $n$  as

$$f_e(c_t^n) = \rho_e(p), \quad (2)$$

where  $\rho_e(p)$  represents the average distance between the blob centroids and their respective epipolar lines as shown in Fig. 4.

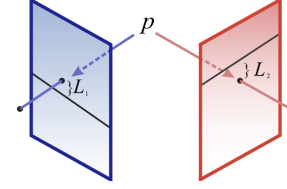


Fig. 4. The epipolar cost of a pairing  $p$  is defined as  $\rho_e(p) = (L_1 + L_2)/2$ .

Suppose  $N$  objects appear in the scene during video capture. Let  $N_t^* \subset \{1, \dots, N\}$  be the set of objects assigned with non-dummy pairings in the current configuration  $C_t$ . The total cost of the configuration based on epipolar constraint is given by

$$f_E(C_t) = \frac{1}{|N_t^*|} \sum_{n \in N_t^*} f_e(c_t^n). \quad (3)$$

To rule out apparent false pairings, we set  $f_e(c_t^n) = \infty$ , if  $\rho_e(c_t^n)$  is greater than a preset threshold  $\epsilon_e$ .

#### 4.2 One-to-one match tendency

Apart from the epipolar constraint, we also measure the level of consistency between the current configuration  $C_t$  and observed blobs by using a criterion based on the following observations: 1) Cameras can be well placed so that they capture most objects simultaneously; 2) at each time step, the proportion of overlapping image blobs on the 2D image plane is relatively small if the density of flying objects is moderate. It indicates that a blob tends to be related to only one object in the scene. This cue also implies that each blob most likely corresponds to only one blob in the other view.

Noticing the tendency of one-to-one match between blobs in different views, we propose two cost functions to penalize missing assignments and duplicate assignments for detected blobs. Given a configuration  $C_t$ , for a blob  $i \in M_t$ , the number of its corresponding blobs in the other view is denoted by  $\tau(i, C_t)$ . The two cost functions are defined as

$$\begin{aligned} f_{C_1}(C_t) &= \frac{1}{|M_t^-|} \sum_{i \in M_t^-} [1 - \tau(i, C_t)] \\ f_{C_2}(C_t) &= \frac{1}{|M_t^+|} \sum_{i \in M_t^+} [\tau(i, C_t) - 1], \end{aligned} \quad (4)$$

where  $M_t^-, M_t^+ \subset M_t$  denotes the sets of blobs that have no corresponding blob and multiple corresponding blobs. According to (4), the configurations having most

blobs corresponding to one blob will have low cost. As shown in Fig. 5, the configuration in (a) better accounts for the blobs detected in each view, and it therefore has lower matching costs.

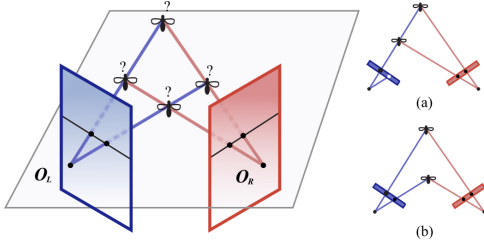


Fig. 5. The configuration in (b) is evaluated as more desirable than the one in (a). Because in (a), repeat assignments and missing assignments make the matching costs high, while in (b), blobs have established one-to-one mapping between views, leading to low matching costs.

### 4.3 Kinetic coherency

Motion tends to be smooth due to limited force against inertia. This continuity can be described by a kinetic model.

Consider a sequence of pairings that have already been assigned to object  $n$  up to time  $t-1$ ,  $c_{1:t-1}^n = (c_1^n, \dots, c_{t-1}^n)$ . At time  $t$ , a pairing  $p$  is to be tentatively assigned to the object  $n$ . To evaluate this assignment  $c_t^n = p$ , we define a motion deviation function  $f_k^{(J)}(p)$  that measures the coherency between the pairing  $p$  and the  $J$  previous pairings  $c_{t-J:t-1}^n$ . If the deviation is small, the assignment is a reasonable one with regard to previous assigned pairings.

Taking all objects into account, the total kinetic coherency at time  $t$  of a given configuration sequence  $C_{1:t} = (C_1, \dots, C_t)$  can be evaluated by

$$f_K^{(J)}(C_t) = \sum_{n=1}^N f_k^{(J)}(c_t^n). \quad (5)$$

At this time, we only consider the case that all objects are present in the scene. In other words, no dummy pairing is assigned to any object. Hence each pairing here corresponds to a 3D position or a pair of 2D positions on image planes. In the following sections, we present several deviation functions  $f_k^{(J)}(\cdot)$  by using different kinds of kinetic models both in 3D space and on 2D image planes.

#### 4.3.1 Kinetic models in 3D space

If the intrinsic and extrinsic parameters are known for each camera, given a pairing, its 3D location can be computed. Consider a sequence of pairings  $c_{1:t}^n = (c_1^n, \dots, c_t^n)$  continuously assigned to object  $n$ . Denote their corresponding 3D locations by  $\mathbf{x}_1, \dots, \mathbf{x}_t$ . We use some kinetic model to predict the 3D locations at time  $t$  from

$J$  previous locations, namely  $\hat{\mathbf{x}}_t = \mathcal{P}(\mathbf{x}_{t-J}, \dots, \mathbf{x}_{t-1})$ . Then the deviation function is defined as

$$f_k^{(J)}(c_t^n) = \|\hat{\mathbf{x}}_t - \mathbf{x}_t\|. \quad (6)$$

Selection of the kinetic model relies on priori knowledge of the motion of the subjects. We adopt here two kinetic models that are prevalently used in tracking moving objects.

The first one is nearest-neighbor model [24]. The nearest-neighbor model depends on only one previous location and uses this location as a prediction for current time, i.e.,  $J = 1$ ,  $\mathcal{P}(\mathbf{x}_{t-1}) = \mathbf{x}_{t-1}$ . The prediction error at time  $t$  for the pairing sequence assigned to object  $n$  is:

$$f_k^{(1)}(c_t^n) = \|\mathbf{x}_t - \mathbf{x}_{t-1}\|. \quad (7)$$

The nearest-neighbor model has been proved to be effective in many tracking applications, particularly when the motion is complex and hard to be formulated, such as wandering people and drifting insects.

The second kinetic model is the smooth-motion model [?]. It is based on the observation that sometimes objects move smoothly due to their inertia. The smoothness indicates their velocities tend to be constant in a local time span. We compute the local velocity from locations at two previous time instances and use it to predict the current location. That is,  $J = 2$ ,  $\mathcal{P}(\mathbf{x}_{t-2}, \mathbf{x}_{t-1}) = 2\mathbf{x}_{t-1} - \mathbf{x}_{t-2}$ . The deviation is then given by

$$f_k^{(2)}(c_t^n) = \|2\mathbf{x}_{t-1} - \mathbf{x}_{t-2} - \mathbf{x}_t\|. \quad (8)$$

#### 4.3.2 Kinetic models on 2D image planes

The kinetic coherency can also be evaluated on image planes by computing the prediction inaccuracies by 2D kinetic model in each view. Consider a sequence of pairings  $c_{1:t}^n = (c_1^n, \dots, c_t^n)$  assigned to object  $n$ . Denote the locations of their blobs in respective views by  $(\mathbf{x}_1^{[1]}, \dots, \mathbf{x}_t^{[1]})$ ,  $(\mathbf{x}_1^{[2]}, \dots, \mathbf{x}_t^{[2]})$ . We define the deviation function on 2D image planes based on nearest-neighbor model as

$$f_k^{(1)}(c_t^n) = \sum_{v \in \{1,2\}} \|\mathbf{x}_t^{[v]} - \mathbf{x}_{t-1}^{[v]}\|. \quad (9)$$

Similarly, the deviation function derived from smooth-motion model is defined as

$$f_k^{(2)}(c_t^n) = \sum_{v \in \{1,2\}} \|2\mathbf{x}_{t-1}^{[v]} - \mathbf{x}_{t-2}^{[v]} - \mathbf{x}_t^{[v]}\| \quad (10)$$

The advantage of using kinetic model on image planes is that it does not require computing the 3D coordinates for each pairing. It therefore enables our framework to be applied in weakly calibrated cases where only fundamental matrices between cameras are known.

### 4.3.3 Kinetic models at initial time steps

Given a pairing sequence  $c_{t_0:t}^n = (c_{t_0}^n, \dots, c_t^n)$ , the deviation can be evaluated only when  $t \geq t_0 + J$  due to the definition of  $f_k^{(J)}(\cdot)$ . We therefore use  $f_k^{(t-t_0)}(\cdot)$  to evaluate pairings at each time step  $t < t_0 + J$ , and we let  $f_k^{(0)}(\cdot) = 0$  at the initial time  $t_0$ .

Since we have prior knowledge that objects move in a way governed by a given kinetic model, it is unnecessary to consider pairing sequences with large deviations from the model. By setting a threshold,  $\epsilon_k$ , if the motion deviation is larger than  $\epsilon_k$ , we let  $f_k^{(J)}(c_t^n) = \infty$  and discard this assignment.

### 4.4 Visibility switching

Since an object may randomly enter and leave the scene, their visibility state could change during the capture process. We use a dummy pairing  $\mathcal{O}$  to represent the absent state of an object. So the problem of changing visibility state can be handled by alternately assigning dummy pairing or non-dummy pairing to the object.

When a dummy pairing and a non-dummy pairing are assigned to the same object at successive time steps, visibility switching happens on this object. We penalize visibility switching by introducing a cost  $\eta$  for each object. To encourage extracting continuous motion trajectories, the value of  $\eta$  is set larger than the motion deviation threshold  $\epsilon_k$  described previously.

Taking the visibility switching into consideration, we evaluate the total kinetic coherency of a configuration sequence  $C_{1:t}$  at time  $t$  by

$$f_K^{(J)}(C_t) = \frac{1}{|N_{t-1}^* \cup N_t^*|} \left[ \sum_{n \in U_t} f_k^{(J)}(c_t^n) + \eta |V_t| \right] \quad (11)$$

instead of (5), where  $N_{t-1}^*, N_t^* \in \{1, \dots, N\}$  denotes objects assigned with non-dummy pairings at the time steps  $t-1$  and  $t$ . The active objects at current time step,  $N_{t-1}^* \cup N_t^*$ , consist of two types of objects. The first type of objects, denoted by  $U_t = (N_{t-1}^* \cap N_t^*)$ , are the objects now present in the scene without changing visibility state at current time step. The second types of objects, denoted by  $V_t = (N_{t-1}^* \cup N_t^*) \setminus U_t$ , refer to the objects now switching the visibility state.

From (11), we can see that visibility switching is expected to happen only when no pairings can be assigned to the object with motion deviation less than  $\epsilon_k$ . Otherwise, keeping the visibility state unchanged and selecting pairings with small motion deviations are more desired.

## 5 COST FUNCTION AND OPTIMIZATION METHOD

Additively combining the above-discussed three cues, we obtain the overall cost function:

$$f(C_{1:T}) = \sum_{t=1}^T [\alpha f_E(C_t) + \beta_1 f_{C_1}(C_t) + \beta_2 f_{C_2}(C_t)] + \gamma \sum_{t=2}^T f_K^{(J)}(C_t) \quad (12)$$

where  $\alpha, \beta_1, \beta_2, \gamma$  are the parameters to control the weights of these terms.

Obtaining the globally optimum result with respect to this cost function requires evaluating all possible configuration sequences in the solution space. Apparently optimization via brute-force enumeration is computationally intractable due to the extremely high dimension of the solution space. Noticing that the cost function can be recursively decomposed into

$$f(C_{1:t}) = f(C_{1:t-1}) + \Delta f(C_t), \quad (13)$$

where the increment of cost  $\Delta f(C_t)$  is

$$\Delta f(C_t) = \alpha f_E(C_t) + \beta_1 f_{C_1}(C_t) + \beta_2 f_{C_2}(C_t) + \gamma f_K^{(J)}(C_t), \quad (14)$$

we are motivated that the cost function can be optimized sequentially through cost propagation. We present an optimization approach base on configuration proposition and cost propagation. It is accomplished iteratively at each time instance by two successive stages: 1) proposing possible configurations for next frame, 2) propagating cumulative cost from previous ones to each newly proposed configuration.

Since the number of possible configurations increases exponentially with the number of objects, it is impossible to list all possible configurations at each time step by brute-force enumeration. It is also unnecessary to enumerate all configurations, because many of them will lead to very high overall cost. Keeping only the configurations with low costs at each time step will tremendously decrease the overall computational cost.

In [45], Gibbs sampling [46] is used to obtain these configurations with low costs by converting the cost function into probability distribution function. But the probability distribution tends to be sparse and contains multiple modes (local peaks), the process is often stacked in a local mode and waste lots of time in sampling configurations of no interest. Instead of using Gibbs sampling, we use a method based on assignment ranking to generate configurations with low costs more efficiently. It is described in the following sections.

### 5.1 Sampling configurations at initial frame

At the first frame, we aim to obtain configurations with the smallest costs according to the cost function  $f(C_1)$ . We denote this sampling process by

$$C_1^{(k)} \sim f(C_1), \quad (15)$$

where  $k = 1, \dots, K$  and  $K$  is the number of configurations we wish to sample. A configuration  $C_1^{(k)}$  is a combination of  $N$  pairings chosen from  $M_1^{[1]} \times M_1^{[2]} \cup \mathcal{O}$ . It is obviously impossible to evaluate all these combinations to acquire the  $K$ -best ones in a reasonable time when the number  $N$  is large.

We know that a blob tends to have one corresponding blob in the other view (Section 4.2). We convert this cue into a one-to-one constraint and impose this constraint on choosing pairings to generate configurations, then the sampling problem becomes obtaining  $K$ -best assignments between the left blobs and the right blobs with the lowest costs in (3). This may cause losses of some possible configurations (some blob may happen to correspond to several blobs in the other view because of occlusion), but it could tremendously reduce the computational costs by avoiding enumerating possible solutions in the entire configuration set.

Let  $a_{ij} \in \{0, 1\}$  be an indicator of the left blob  $i$  being assigned to the right blob  $j$  (1 for true, 0 for false). Denote the pairing composed of these blobs by  $p$ . The cost of blob  $i$  being assigned to blob  $j$  is given by  $c_{ij} = \rho_e(p)$ . Denote the number of blobs in each view by  $S_1, S_2$ . Without loss of generality, here we assume that  $S_1 \leq S_2$ . Thus an assignment  $\mathbf{a} = (a_{ij})$  should satisfy the following conditions

$$\sum_{j=1}^{S_2} a_{ij} = 1, i = 1, \dots, S_1 \text{ and } \sum_{i=1}^{S_1} a_{ij} \leq 1, j = 1, \dots, S_2$$

$$a_{ij} \geq 0. \quad (16)$$

Our goal is to obtain the  $K$ -best assignments that have the lowest costs of

$$\sum_i \sum_j a_{ij} c_{ij}. \quad (17)$$

This is an assignment ranking problem that can be solved by Murty's algorithm [47], of which the computational complexity is  $O(K \cdot N^4)$ ,  $N$  here is  $S_1$ . Using the improved algorithms described in [48] [49], the computational complexity could reduce to  $O(K \cdot N^3)$ .

By solving the assignment ranking problem,  $K$  configurations of high interests can be acquired. For each sampled configuration, we use (12) to compute its cost. Tree-like data structure is used to store sampled configurations. The configurations sampled at the initial frame are stored at the roots of these trees. The trees grow when configurations at the next frame are sampled from the parent configuration frame by frame. In the next stage, we described how to iteratively sample the subsequent configurations of the current configuration and evaluate their cumulative costs.

## 5.2 Sampling child configurations at the next frame

For each configuration at current time step  $t-1$ , we can obtain a sequence of configurations by traveling back to

the root of the tree. Denote the configuration sequence by  $C'_{1:t-1}$ . We attempt to expand the tree by sampling an configuration of low incremental cost, namely,

$$C_t^{(k)} \sim \Delta f(C_t). \quad (C_{1:t-1} = C'_{1:t-1}). \quad (18)$$

Although the incremental cost relies all three cues as shown in (14), we achieve the goal of sampling configurations of high interests in a greedy way: we first try to obtain configurations that having low costs of epipolar constraint and kinetic coherency; we then adjust newly obtained configurations by enforcing each of them to satisfy the one-to-one match criterion to reduce the incremental cost.

As we know in Section 4.4, keeping visibility unchanged will lead to low kinetic cost defined in (11). The first step is to assign the objects assigned with non-dummy pairings in  $C'_{t-1}$  to the possible true pairings with infinity epipolar costs (2). The cost of assigning  $i$ -th object to  $j$ -th pairing is given by

$$c_{ij} = \alpha f_e(c_t^i) + \gamma f E_k^{(J)}(c_t^i) \quad (c'_{1:t-1} = c'_{1:t-1}). \quad (19)$$

Here  $c_t^i$  represents the  $j$ -th pairing assigned to the  $i$ -th object. This is also an assignment problem as stated in the pervious section. We also obtain the  $K$ -best assignments by using assignment ranking algorithms.

Sometimes in some acquired assignments, the pairing assigned to an object could lead to a large kinetic deviation greater than a preset threshold, namely,  $f_k^{(J)}(c_t^i) > \epsilon_k$ . In this situation, the object is much likely to be absent from the scene at that time, so we replace the assigned pairing of this object with the dummy pairing  $\mathcal{O}$  instead. The replacement is reasonable since it could reduce the kinetic cost. From these assignments,  $K$  configurations can be constructed by filling each dimension related to these objects with assigned pairings.

The second step is to recompose the newly acquired configurations so as to make the resulting configurations satisfy the constraint of one-to-one match. Let  $M^{[1]-}$  and  $M^{[2]-}$  be the sets of blobs corresponding to no object in respective views. To decrease the costs derived from the one-to-one match cue, we try to assign pairings into the set of  $M^{[1]-} \times M^{[2]+}$  to the unassigned objects in  $N^- = N \setminus N^*$ . The task can be done exactly in the same way as in sampling configurations at the initial frame. By solving the assignment ranking problem,  $K'$  combinations of pairings with the smallest epipolar errors are obtained. Each combination corresponds to a scheme of assigning pairings in  $M^{[1]-} \times M^{[2]-}$  to the unassigned objects in  $N^-$ . After that, the  $K$  configurations acquired in the previous step are recomposed to generate  $K \times K'$  new configurations, each of which has very low incremental costs of (14).

## 5.3 Pruning and cost propagation

The cumulative cost of a newly sampled configuration  $C_t^{(k)}$ , denoted by  $f^*(C_t^{(k)})$ , which is the cost of the



configuration sequence in the path from the tree root to the current leaf, is recursively computed from its parent configuration,  $C_{t-1}^{(k')}$ , namely,  $f^*(C_t^{(k)}) = f^*(C_{t-1}^{(k')}) + \Delta f(C_t^{(k)})$ . The cost of the tree root at the first frame is directly evaluated by using (12).

As the number of configurations increase exponentially when the trees grow over time, we prune the configurations with high cumulative costs at each frame and keep the number of remaining configurations in a reasonable level. Configuration sampling and cost propagation are performed frame by frame and finally the optimum configurations can be acquired by tracing back from the configuration with the lowest cumulative cost to the tree root at the first frame, as shown in Fig. 6.

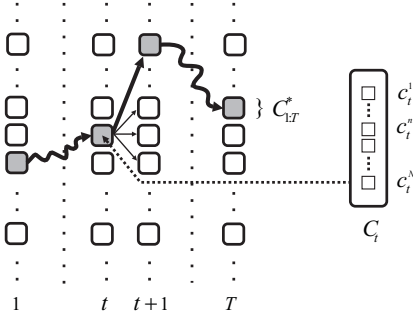


Fig. 6. Optimization is done by sampling new configurations at next frame and propagating cumulative costs to them until reaching the last frame. Finally the optimum configurations sequence  $C_{1:T}^*$  is obtained by tracing back from the configuration with the smallest cumulative cost.

When the optimum configuration sequence  $C_{1:T}^*$  is acquired, 3D motion trajectories can be computed from the pairing sequence in each dimension of  $C_{1:T}^*$ . Notice that a pairing sequences could contain some dummy pairings. These dummy pairings separate the whole pairing sequence into several non-dummy pairing segments. The motion trajectories are recovered at each of these segments for corresponding objects.

#### 5.4 Parameters setting

The variables  $\alpha, \beta_1, \beta_2$ , and  $\gamma$  are four basic parameters in our algorithm, which control the weights of the four components in the cost function. We define three variables  $\phi_e, \phi_c$ , and  $\phi_k$  to normalize the four components into the same order of magnitude. Then we use four relative weights  $\tilde{\alpha}, \tilde{\beta}_1, \tilde{\beta}_2$ , and  $\tilde{\gamma}$  that  $\alpha = \tilde{\alpha}/\phi_e, \beta_1 = \tilde{\beta}_1/\phi_c, \beta_2 = \tilde{\beta}_2/\phi_c$ , and  $\gamma = \tilde{\gamma}/\phi_k$  to exercise influence on the respective costs. Here we set  $\phi_e = \epsilon_e$  and  $\phi_k = \epsilon_k$ . The value of  $\phi_c$  depends on the density of objects moving in the scene. It is set several times larger than the average number of corresponding objects of each projection on the image plane.

The threshold value of  $\epsilon_e$  depends on the object detection error and calibration error in the capturing system. Smaller  $\epsilon_e$  could lead to less possible pairings and

therefore reduce the running time for optimization, but it requires more accurate object detection and calibration. The kinetic deviation threshold  $\epsilon_k$  can be determined in an automatic way. For each pairing, we compute the distance to its nearest pairing at the next frame using the distance functions between pairings as in (7) or (9). Denoting the average nearest distance of all pairings by  $\bar{\mathcal{D}}$ , the threshold  $\epsilon_k$  can be set empirically several times larger than  $\bar{\mathcal{D}}$ , namely  $\epsilon_k = r_k \cdot \bar{\mathcal{D}}$ , where  $r_k > 1.0$ .

The visibility switching cost  $\eta$  is set to be larger than the kinetic deviation threshold  $\epsilon_k$  to prevent undesired visibility switching, which usually breaks the continues trajectories into pieces. The remaining parameters  $K$  and  $\tilde{K}$  are the number of configurations sampled at each sampling step and the maximum number of configurations retained at each time instance. They are desirable to be large so as to produce more favorable result, but not be exceedingly large because of the limitation of the computational capability of hardware.

## 6 EXPERIMENTS

We have carried out experiments using simulated particle swarms and real-world fruit flies (*Drosophila melanogaster*). In the experiment of simulated swarms, the proposed method was compared with other strategies under different settings, including various density, velocity, and trajectory smoothness. Since the ground truth was known, the performance was compared in a quantitative way. In the fruit fly experiment, we recovered the 3D motion trajectories of a large group of flying fruit flies. The performance was evaluated against visual inspection as the ground truth was unavailable.

### 6.1 Simulated particle swarms

*Data generation:* The particles are confined in a cube of size  $1.0m \times 1.0m \times 1.0m$ . Each particle is initialized with a random location and assigned a velocity of random direction and constant magnitude  $v$ . At each time step, the direction of the velocity vector is updated by adding a random vector  $\delta \mathbf{n}$  followed by normalization to make the vector of unit length, that is

$$\mathbf{n}_t = \frac{\theta \mathbf{n}_{t-1} + (1 - \theta) \delta \mathbf{n}}{\|\theta \mathbf{n}_{t-1} + (1 - \theta) \delta \mathbf{n}\|}, \quad (20)$$

The parameter  $\theta \in [0, 1]$  is used to control the smoothness of the trajectory as shown in Fig. 7. Each element of  $\delta \mathbf{n}$  is uniformly drawn from  $[-1.0, 1.0]$ . The resultant velocity vector is then updated by

$$\mathbf{v}_t = (v_{t-1} + s_t) \mathbf{n}_t. \quad (21)$$

$s_t \sim \text{where } \mathcal{N}(0, 0.05)$  is a Gaussian noise used to slightly perturb the velocity magnitude.

After the velocity vector is obtained, the location of the object is computed from previous location via  $\mathbf{x}_t = \mathbf{x}_{t-1} + \mathbf{v}_t \cdot \Delta t$ . The objects keep on moving until they hit the boundaries of the cube, where they bounce back.

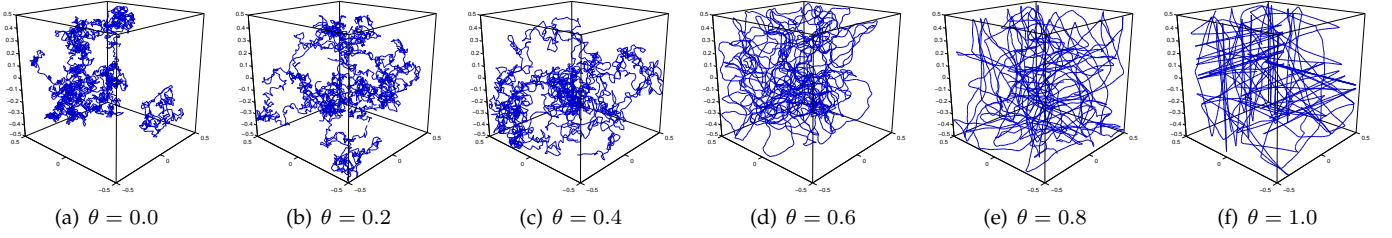


Fig. 7. Trajectories generated with different  $\theta$

The scene is rendered using OpenGL frame by frame to produce video sequences for the experiment. We use two virtual cameras of resolution  $800 \times 800$  to capture the scene. Each test sequence contains 100 video frames and each object is rendered as a sphere. The radius of each sphere is set to 0.005 producing image blobs of average diameter of 6 pixels.

We then treat the generated video sequences as input and detect the blobs and compute their centers. To simulate detection and calibration errors that exist in real-world cases, the obtained coordinates are perturbed by random noise drawn from a Gaussian distribution  $s \sim \mathcal{N}(0, 1.0)$  (pixel) (for both X and Y).

**Evaluation metrics:** The first step of evaluating performance is to match reconstructed trajectories  $\{r_1, \dots, r_m\}$  to ground truth trajectories  $\{g_1, \dots, g_n\}$ . A reconstructed trajectory is regarded as well matched to a ground truth trajectory if the coordinates of the reconstructed trajectory are nearly identical to those of the ground truth trajectory over the entire track. Denote the position of  $r_i$  at time  $t$  by  $r_i^t$  and the position of  $g_j$  at time  $t$  by  $g_j^t$ . If  $|r_i^t - g_j^t| < \kappa$  for all time steps within the time duration of  $r_i$ , then  $r_i$  is said to be well matched to  $g_j$  and the trajectory  $r_i$  is said to be *correct*. The threshold  $\kappa$  is used to allow for numerical inaccuracy. If a correct trajectory has the same time duration as that of the corresponding ground truth trajectory, it is also *complete*. The unmatched trajectories are false ones.

The evaluation is performed by assessing three aspects of the result : 1) the proportion of correct trajectories (*correctness*) ; 2) among these correct trajectories, how many of them are complete (*completeness*); 3) the amount of false trajectories (*precision*).

Let  $\mathcal{L}_g$  denote the total length of ground truth trajectories and  $\mathcal{L}_c$  represent the length of correct trajectories. A metric (*CT*) is defined to measure the level of *correctness*, namely,

$$CT = \mathcal{L}_c / \mathcal{L}_g. \quad (22)$$

A higher value of *CT* indicates more correct trajectories are obtained. *CT* approaching to 1 indicates all the ground truth trajectories are correctly reconstructed. The *completeness* of the result is evaluated by

$$CP = n_c / n_g, \quad (23)$$

where  $n_c$  denotes the number of complete trajectories,  $n_g$  is the number of ground truth trajectories. It is

insufficient to use only *CT* and *CP* to evaluate the result, since the result with high *CT* and *CP* could still be undesirable, i.e. , some of the reconstructed trajectories do not exist in the ground truth (false trajectories). So the result is further evaluated by the *precision* metric (*PR*), defined as

$$PR = \mathcal{L}_c / \mathcal{L}_r. \quad (24)$$

*PR* measures the proportion of the correct trajectories out of all reconstructed trajectories. A high *precision* indicates that few false trajectories are generated. Ideally, if all trajectories are correctly reconstructed and no false trajectory exists, all metrics reach up to the maximum value 1.0.

**Methods for comparison:** Although there is no existing method highly effective for reconstructing 3D motion trajectories of particle swarms, we implement several of them using three typical strategies to compare with the proposed method. They are Reconstruction-Tracking method, Tracking-Reconstruction method, and Tracking-Reconstruction-Stitching method.

In Reconstruction-Tracking (RT) method, 3D coordinates are reconstructed at each frame and the 3D motion trajectories of the objects are then obtained via tracking in 3D space. The stereo correspondence between image objects across views is established by solving a linear assignment problem that minimize overall epipolar error. For tracking in the 3D space, the state-of-the-art methods for tracking point-like objects, GOA tracker, is used.

In Tracking-Reconstruction method (TR), objects are tracked on the image plane of each view; the corresponding 2D trajectories are then matched by examining if their coordinates continuously satisfy the epipolar constraint over the entire track [19]. After that, 3D trajectories are reconstructed from each pair of matched 2D trajectories. We use GOA tracker to track these 2D particle-like objects.

The Tracking-Reconstruction-Stitching (TRS) method is an improvement of the Tracking-Reconstruction method. In TRS, we do not attempt to track objects throughout the entire duration since the presence of tracking ambiguity could lead to incorrect tracking results. Instead, we track objects only in a local time span when no tracking ambiguity exists - the object under tracking keeps a considerable distance away from others at that time. Then stereo matching is proceeded on these 2D trajectory segments obtained by partial tracking to

yield trajectory segments in 3D space. In the final stage, these 3D trajectory segments are stitched together to generate complete trajectories.

### 6.1.1 Experiment with various object density

In this experiment, we analyze the performance of the proposed method with respect to object density. The speed magnitude is set to  $v = 0.02$ , and the smoothness parameter is set to  $\theta = 0.7$ . The number of objects present in the scene increases from 20 to 150 at a step of 10.

We generate three data sets for each density and obtain the average performance. Four different kinetic models described in equations (7), (8), (9), and (10) (NN, SM, IMNN, IMSM for short respectively) are adopted for the test. In the TR method, we use GOA tracker with smooth motion model to track trajectories on the 2D image planes. The maximum number of video frames allowed for stitching and interpolation for the TRS method is set to 10.

The comparison results are shown in Fig. 8. Compared with the RT method, the TR method achieved a better *CP*, which means it produces more complete trajectories than the RT method does. The TR method however has a much lower *CT*. This is because the TR method heavily relies on the 2D tracking performance. Incorrect 2D tracks will cause matching failure and loss of 3D trajectories. The TR method nevertheless seldom generate false trajectories ( see the result produced by the TR method in Fig. 10). So the TR method gained a high *PR* as shown in Fig. 8(c).

The TRS method performed better than the TR method and the RT method. The performance achieved by the TRS method declines quickly when the density rises. This is due to two reasons: 1) when the density rises, the 2D track segments are too short to eliminate stereo matching ambiguities; 2) it is difficult to connect the broken trajectories because of the long time durations of the missing pieces.

The results show that the proposed method performed best among the compared methods. When the number of objects reached 150, *CP* declined to 0.6, while *CT* and *PR* of the result were still greater than 0.85. The high *CT* and *PR* value indicates that if some extrapolation processes are adopted, the performance of the proposed method can be further improved - more complete trajectories can be obtained. A visual comparison of the various methods is also given in Fig. 10.

### 6.1.2 Experiment with various velocity

We change the mean velocity by modifying the velocity magnitude  $v$  from 0.01 per video frame to 0.05 per video frame. The number of objects in the scene is set to 70. The smoothness parameter  $\theta$  is set to 0.7. At each step, the velocity magnitude increases by 0.005, and three data sets are generated to gauge the average performance. Smooth motion models (SM, IMSM) are adopted for the proposed method. The parameter settings of the

methods for comparison are the same as those in the previous experiment.

The results are shown in Fig. 9. As the average velocity of moving particles increases, the performance of the methods for comparison drop dramatically. When the velocity rises greater than 0.02 (the particle travels two times its diameter between two adjacent frames), no complete trajectory could be generated by these methods. The proposed method however performed remarkably better than all these methods. It still successfully reconstructed 80 percent of the ground truth trajectories and generates less than 20 percent of incomplete or incorrect trajectories when the velocity reaches to 0.05 per frame. This shows the strong capability of the proposed method in handling video sequences of low frame rates with respect to the velocity of the fast moving objects.

### 6.1.3 Experiment with various smoothness

The trajectory smoothness is controlled by the parameter  $\theta$  as discussed in Section 6.1. We set the number of objects in the scene to 50 and change the smoothness by adjusting the parameter  $\theta$  from 0.1 to 1.0 at a step of 0.1. Three data sets are generated to gauge the average performance for each  $\theta$  value.

This experiment gives results under two velocity,  $v = 0.01$ ,  $v = 0.04$ , as shown in Fig. 11. The results indicate that when the average speed of moving objects is high, selecting a proper kinetic model for reconstruction of trajectories of specific smoothness plays an important role in gaining better performance. But in low speed cases, the choice of kinetic models has less influence on the performance. As shown in Fig. 11, when the average velocity is 0.01, the method adopting two different kinetic models produced similar performance.

## 6.2 Fruit fly swarm

Fruit fly (*Drosophila Melanogaster*) is a model organism extensively used in genetic research since Thomas Hunt Morgan founded his famous Fly Room in 1910 [50]. It is also an important subject for animal behavior research. Existing studies have been conducted on the behavior of an individual fly or the interaction of a small number of flies during sleep and courtship [51], while the behavior in a large group context has been little studied.

Although fruit fly is less well known for their social interaction than classic eusocial insects such as bees and ants, their collective behavior has attracted increasing attention recently. A recent editorial [52], for example, has pointed out “*methods to study the behavior of Drosophila sp. in the context of a group may deepen our understanding of the neural mechanisms underlying social behavior*”.

There are many interesting questions waiting to be addressed: How do fruit flies interact among themselves? Is there any communication among them during flight? How do they avoid collisions when they are hovering in a dense aggregation? To answer such questions, the ability to measure the 3D motion trajectories of the

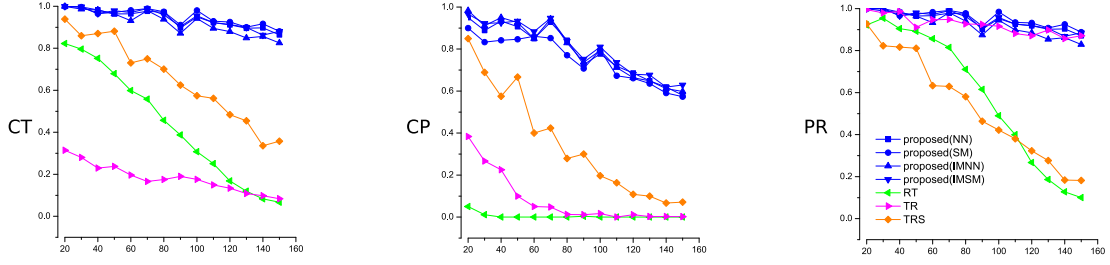


Fig. 8. Results for various object density.

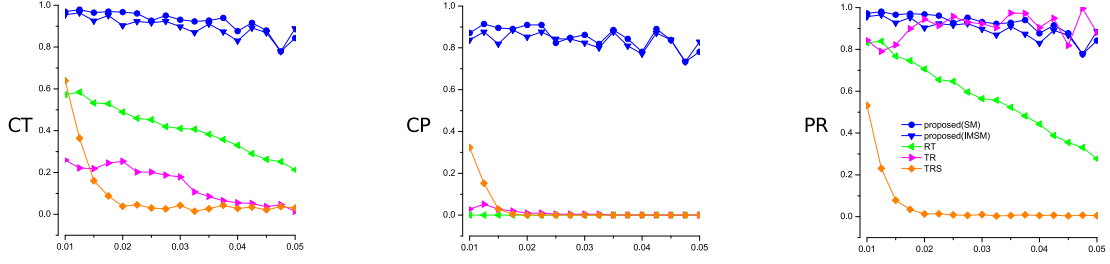


Fig. 9. Results for variable velocity.

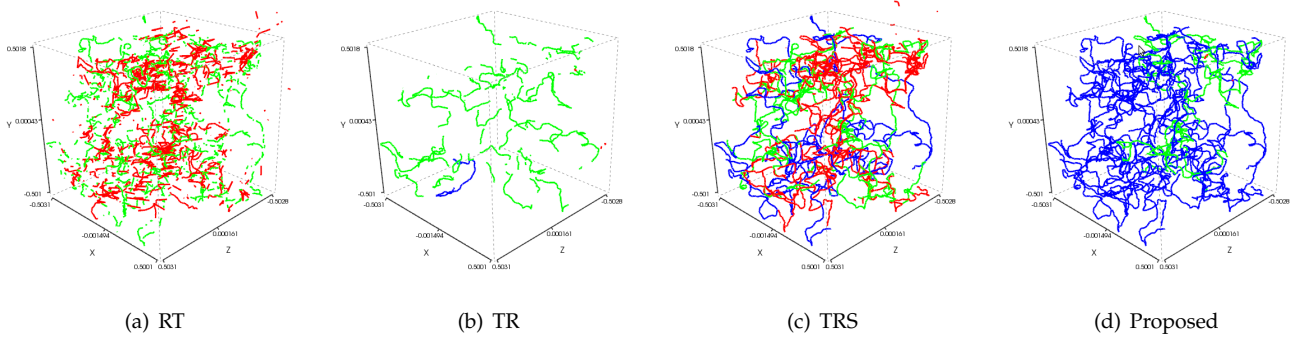


Fig. 10. A visual comparison of different methods ( $\theta = 0.7$ ,  $v = 0.02$ , 80 objects). The blue ones show complete and correct trajectories; the green curves show *correct* trajectories; the blue ones represent the *complete* trajectories; the red ones are *fake* trajectories.

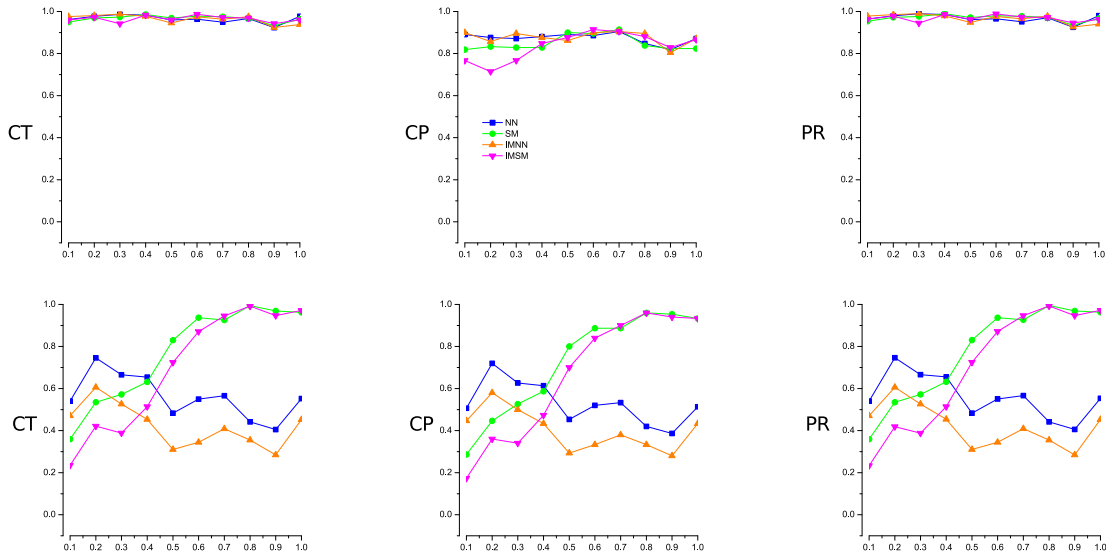


Fig. 11. The results of different smoothness under two velocities - first row (0.01) and second row (0.04).



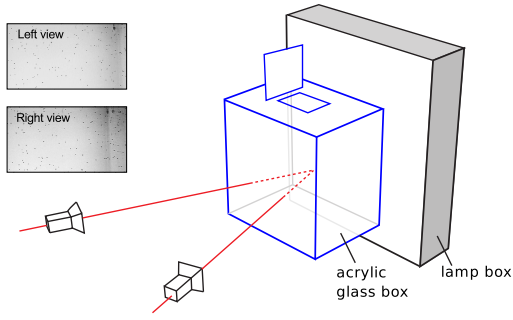


Fig. 12. The two camera system for fruit flies.

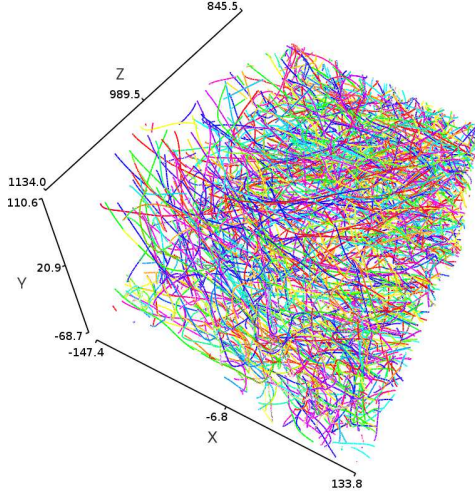


Fig. 13. The reconstruction results from a pair of stereo video streams of 1000 frames : 1105 fly trajectories are reconstructed over a 5 second period. The axis unit is *mm*.

individuals is of key importance. This is therefore our motivation to reconstruct 3D motion trajectories of a swarm of flying fruit flies.

Computer vision techniques had been used to acquire the 3D trajectories of flying flies in [39], [53]. They however mainly focused on the study of the flight performance of an individual fruit fly and their systems captured only a few flies. We set up a two camera system and applied the proposed approach to acquire the 3D trajectories of hundreds of flying fruit flies.

Our experiment system for fruit flies is illustrated in Fig. 12. The fruit flies flew in an acrylic glass box of size  $35\text{cm} \times 25\text{cm} \times 35\text{cm}$  (height), where the background was uniformly illuminated by a lamp box consisting of 6 fluorescent tubes and a frosted surface. To avoid flickering, these tubes were powered by a direct current supplier. Two Sony HVR-V1a video cameras, working in the high speed mode of 200 frame per second, were used to capture the scene from two different views. The image resolution was  $960 \times 540$ . The two cameras were temporally synchronized and geometrically calibrated.

We applied background subtraction technique to detect the fruit flies and then computed their centers. We

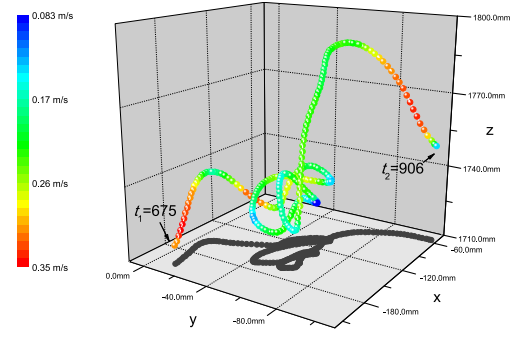


Fig. 14. The trajectory of a single fly entering the scene at the 675-th frame and leaving at the 906-th frame. Six saccades [54] occurred along the path.

then applied our method to reconstruct the 3D trajectories of a sequence of 1000 frames (5 seconds). The results are given in Fig. 13, showing 1105 reconstructed trajectories.

We tried to establish the ‘ground truth’ through manually tracking the flies on image planes and then matching these 2D trajectories to generate the trajectories of flies, but found that the task was too difficult even for human vision (Fig. 17). We therefore evaluated the results by viewing the results both in 3D coordinate system and 2D image planes frame by frame (Fig. 17). Through observation, we found that most of trajectories were reconstructed correctly and completely. We counted the incomplete trajectories that suddenly appeared or disappeared in the field of view and found that on average about 2.3% trajectories at each frame were incomplete.

Fig. 15(a) shows the average length of reconstructed trajectories up to that time at each frame. For comparison, we also gave the result generated by the TRS method (the best one among the existing methods as shown in previous sections). We can see that the average trajectory lengths of the proposed method are much longer than those of the TRS method, which indicates more trajectories are correctly reconstructed, as false trajectories seldom have long duration because of the epipolar motion [19]. The number of reconstructed flies and the number of detected flies on the image plane (the minimum among the two cameras) at each frame are shown in Fig. 15(b). The result indicates most flies are successfully tracked except that a few flies might be captured by only one camera (such as unmarked flies near image boundaries in Fig. 18(a)/(b)). The performances of the TRS method are also presented in Fig. 15. It can be seen that the proposed method exhibits a remarkable advantage over the TRS method.

Fig. 17 shows tracking results of the proposed method on the image plane. The flies moved closely to each other or overlapped frequently. In such situation, it is extremely difficult to yield the trajectories of flies by using object tracking techniques on the 2D image plane or even by manually labeling. The proposed method, however, can easily maintain the identities of flies over time, in



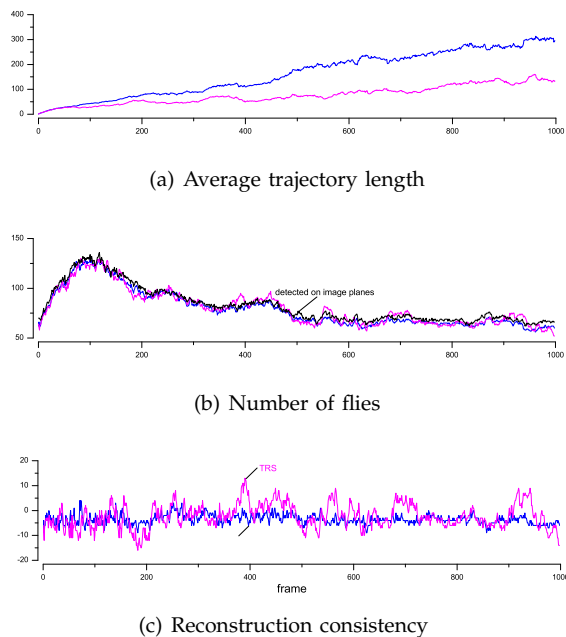


Fig. 15. (a) The average trajectory length at each frame (up to that time step). (b) The number of reconstructed flies and the number of detected flies on the image planes (the smaller one between two cameras). (c) The reconstruction consistency is measured by the difference between the number of reconstructed 3D flies and the one detected on image planes. The variance of number difference of the proposed method is 4.15, while the one of the TRS method is 23.98, indicating the number of flies reconstructed by the proposed method are more consistent with flies present in video sequences.

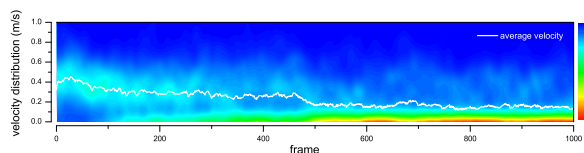


Fig. 16. The velocity distribution of the flies at each frame. Notice that the velocities of flies decline when time passes by. This is because flies tend to land on the wall of the glass box after a period of flying.

spite of the existence of severe tracking ambiguities.

## 7 CONCLUSION

We have developed a novel approach to measuring the 3D motion trajectories of large swarm of moving objects of identical appearance by using two cameras. Unlike the existing methods, the proposed method unifies tracking and stereo matching into a single cost optimization problem, mitigating the ambiguities encountered by each of them. Experimental results show clear advantage of the proposed method over the existing methods.

We have used the proposed method to reconstruct 3D motion trajectories of a large group of flying fruit flies.

To our best knowledge, this is the first time that the 3D motion trajectories of a large swarm of flying insects are successfully obtained. With these trajectories, the kinetic information of the flies can be computed. e.g. We can extract velocity distribution of the flying flies at each frame as shown in Fig. 16, and analyze a single trajectory to study the individual flight behavior as shown in Fig. 14. The availability of 3D motion trajectories of each individual of a flying swarm provides an opportunity of quantitative analysis for behavior study.

## ACKNOWLEDGMENTS

The research work presented in this paper is supported by National Natural Science Foundation of China, Grant No. 60875024, Education Commission of Shanghai Municipality Grant No. 10ZZ03, and Science and Technology Commission of Shanghai Municipality, Grant No. 09JC1401500.

## REFERENCES

- [1] J. Emlen Jr, "Flocking behavior in birds," *The Auk*, vol. 69, no. 2, pp. 160–170, 1952.
- [2] T. Pitcher, "Behaviour of Teleost Fishes." *Fish and Fisheries Series*, 1993.
- [3] L. Taylor, "Insect migration, flight periodicity and the boundary layer," *The Journal of Animal Ecology*, vol. 43, no. 1, pp. 225–238, 1974.
- [4] J. Reichard, L. Gonzalez, C. Casey, L. Allen, N. Hristov, and T. Kunz, "Evening emergence behavior and seasonal dynamics in large colonies of Brazilian free-tailed bats," *Journal of Mammalogy*, vol. 90, no. 6, pp. 1478–1486, 2009.
- [5] J. Kennedy, "Swarm intelligence," *Handbook of Nature-Inspired and Innovative Computing*, pp. 187–219, 2006.
- [6] C. Reynolds, "Flocks, herds and schools: A distributed behavioral model," in *Proceedings of the 14th annual conference on Computer graphics and interactive techniques*. ACM, 1987, pp. 25–34.
- [7] A. Jadbabaie, J. Lin, and A. Morse, "Coordination of groups of mobile autonomous agents using nearest neighbor rules," *IEEE Transactions on Automatic Control*, vol. 48, no. 6, pp. 988–1001, 2003.
- [8] R. De Nardi, O. Holland, J. Woods, and A. Clark, "SwarMAV: A swarm of miniature aerial vehicles," in *Proceedings of the 21st Bristol International UAV Systems Conference*. Citeseer, 2006.
- [9] R. Cont and J. Bouchaud, "Herd behavior and aggregate fluctuations in financial markets," *Macroeconomic dynamics*, vol. 4, no. 02, pp. 170–196, 2000.
- [10] D. Helbing, I. Farkas, and T. Vicsek, "Simulating dynamical features of escape panic," *Nature*, vol. 407, no. 6803, pp. 487–490, 2000.
- [11] T. Vicsek, A. Czirók, E. Ben-Jacob, I. Cohen, and O. Shochet, "Novel type of phase transition in a system of self-driven particles," *Physical Review Letters*, vol. 75, no. 6, pp. 1226–1229, 1995.
- [12] I. Couzin, J. Krause, R. James, G. Ruxton, and N. Franks, "Collective memory and spatial sorting in animal groups," *Journal of Theoretical Biology*, vol. 218, no. 1, pp. 1–11, 2002.
- [13] J. Parrish and L. Edelstein-Keshet, "Complexity, pattern, and evolutionary trade-offs in animal aggregation," *Science*, vol. 284, no. 5411, p. 99, 1999.
- [14] M. Nagy, Z. Ákos, D. Biro, and T. Vicsek, "Hierarchical group dynamics in pigeon flocks," *Nature*, vol. 464, no. 7290, pp. 890–893, 2010.
- [15] N. KASAGI and K. NISHINO, "Probing turbulence with three-dimensional particle-tracking velocimetry," *Experimental thermal and fluid science*, vol. 4, no. 5, pp. 601–612, 1991.
- [16] N. Malik, T. Dracos, and D. Papantoniou, "Particle tracking velocimetry in three-dimensional flows - part ii: particle tracking," *Experiments in Fluids*, vol. 15, no. 4, pp. 279–294, 1993.
- [17] F. Pereira, H. Stuer, E. Graff, and M. Gharib, "Two-frame 3d particle tracking," *Measurement Science and Technology*, vol. 17, no. 7, pp. 1680–1692, 2006.

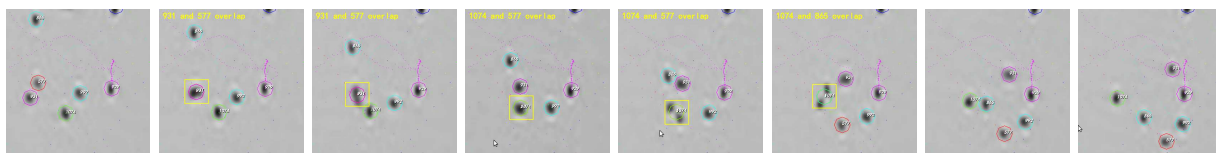


Fig. 17. The fly trajectories on the 2D image plane resulted from the proposed method, where each fly was labeled with a unique number. These flies moved closely to each other or overlapped frequently, which causes extreme difficulty to establish correct temporal correspondences even by manually labeling.

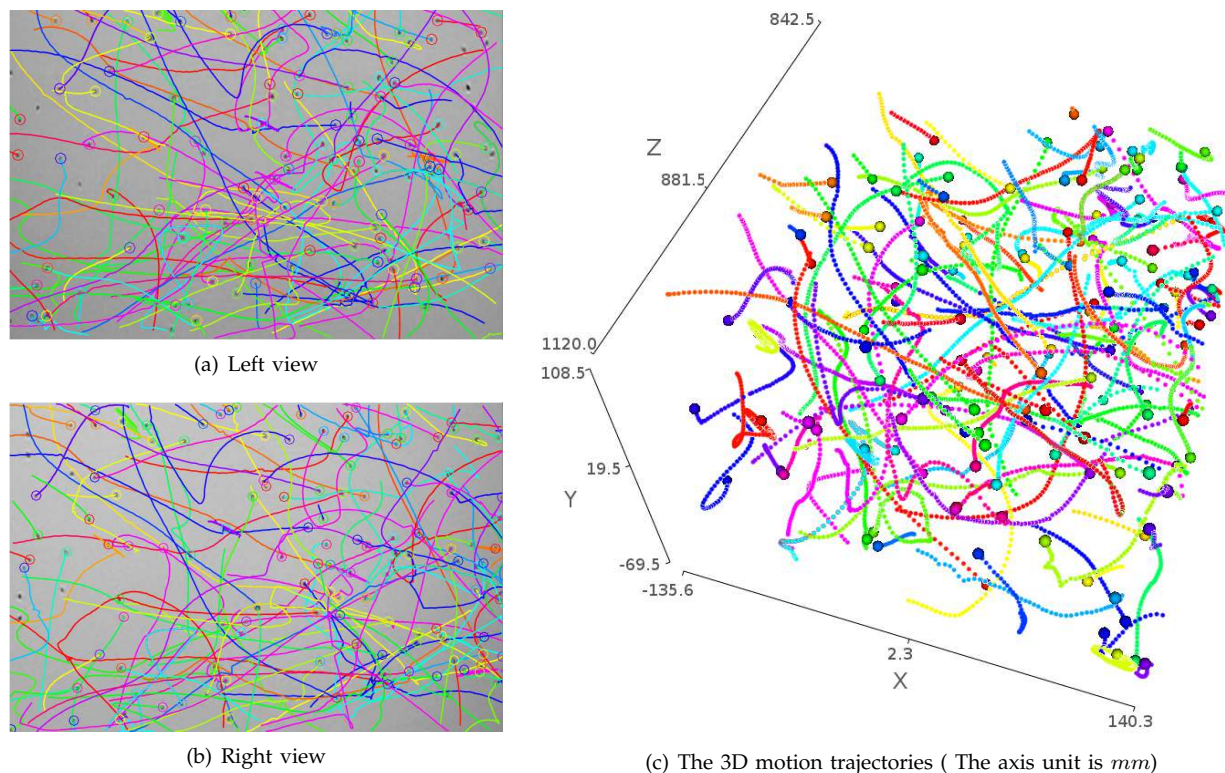


Fig. 18. The current frame here is 96. The corresponding flies both on image planes and in 3D space are marked by the same color.

- [18] D. Grover, J. Tower, and S. Tavaré, "O fly, where art thou?" *Journal of The Royal Society Interface*, vol. 5, no. 27, p. 1181, 2008.
- [19] H. Du, D. Zou, and Y. Chen, "Relative epipolar motion of tracked features for correspondence in binocular stereo," in *IEEE International Conference on Computer Vision*, 2007.
- [20] Y. Guezennec, R. Brodkey, N. Trigui, and J. Kent, "Algorithms for fully automated three-dimensional particle tracking velocimetry," *Experiments in Fluids*, vol. 17, no. 4, pp. 209–219, 1994.
- [21] D. Engelmann, C. Garbe, and M. Stöhr, "Stereo particle tracking," in *Proc. of 8th Int. Symp. on Flow Visualization (CD-ROM)*, 1998, pp. 240–1.
- [22] D. Reid, "An algorithm for tracking multiple targets," *IEEE Transactions on Automatic Control*, vol. 24, no. 6, pp. 843–854, 1979.
- [23] T. Fortmann, Y. Bar-Shalom, M. Scheffe, B. Beranek, I. Newman, and M. Cambridge, "Sonar tracking of multiple targets using joint probabilistic data association," *IEEE Journal of Oceanic Engineering*, vol. 8, no. 3, pp. 173–184, 1983.
- [24] C. Veenman, M. Reinders, and E. Backer, "Resolving motion correspondence for densely moving points," *IEEE Transactions on Pattern Analysis and Machine Intelligence*, pp. 54–72, 2001.
- [25] N. Gordon, D. Salmond, and A. Smith, "Novel approach to nonlinear/non-gaussian bayesian state estimation," in *IEE Proceedings*, vol. 140, no. 2, 1993, pp. 107–113.
- [26] R. Danchick and G. Newnam, "A fast method for finding the exact n-best hypotheses formultitarget tracking," *IEEE Transactions on Aerospace and Electronic Systems*, vol. 29, no. 2, pp. 555–560, 1993.
- [27] I. Cox and S. Hingorani, "An efficient implementation of reid's multiple hypothesis trackingalgorithm and its evaluation for the purpose of visual tracking," *IEEE Transactions on Pattern Analysis and Machine Intelligence*, vol. 18, no. 2, pp. 138–150, 1996.
- [28] C. Hue, J. Le Cadre, P. Perez, and R. IRISA, "Tracking multiple objects with particle filtering," *IEEE Transactions on Aerospace and Electronic Systems*, vol. 38, no. 3, pp. 791–812, 2002.
- [29] J. MacCormick and A. Blake, "A probabilistic exclusion principle for tracking multiple objects," *International Journal of Computer Vision*, vol. 39, no. 1, pp. 57–71, 2000.
- [30] J. Willneff and A. Gruen, "A new spatio-temporal matching algorithm for 3d-particle tracking velocimetry," in *The 9th International Symposium on Transport Phenomena and Dynamics of Rotating Machinery*, Honolulu, Hawaii, USA, February, 2002, pp. 10–14.
- [31] Z. Khan, T. Balch, and F. Dellaert, "Mcmc-based particle filtering for tracking a variable number of interacting targets," *IEEE Transactions on Pattern Analysis and Machine Intelligence*, pp. 1805–1918, 2005.
- [32] A. Veeraraghavan, R. Chellappa, and M. Srinivasan, "Shape-and-behavior encoded tracking of bee dances," *IEEE Transactions on Pattern Analysis and Machine Intelligence*, vol. 30, no. 3, pp. 463–476, 2008.
- [33] D. Tweed and A. Calway, "Tracking many objects using subordinated condensation," in *British Machine Vision Conferenc*. Citeseer, 2002.
- [34] M. Betke, D. Hirsh, A. Bagchi, N. Hristov, N. Makris, and T. Kunz,

- "Tracking large variable numbers of objects in clutter," in *IEEE Conference on Computer Vision and Pattern Recognition*, 2007, pp. 1–8.
- [35] K. Branson, A. Robie, J. Bender, P. Perona, and M. Dickinson, "High-throughput ethomics in large groups of drosophila," *Nature methods*, vol. 6, no. 6, pp. 451–457, 2009.
  - [36] H. Buelthoff, T. Poggio, and C. Wehrhahn, "3-d analysis of the flight trajectories of flies (*drosophila melanogaster*)," *Zeitschrift für Naturforsch.*, vol. 35, pp. 811–815, 1980.
  - [37] C. Wehrhahn, T. Poggio, and H. Bülthoff, "Tracking and chasing in houseflies (*musca*). an analysis of 3-d flight trajectories." *Biological Cybernetics*, vol. 45, no. 2, pp. 123–130, 1982.
  - [38] J. Rayner and H. Aldridge, "Three-dimensional reconstruction of animal flight paths and the turning flight of microchiropteran bats," *Journal of Experimental Biology*, vol. 118, no. 1, pp. 247–265, 1985.
  - [39] G. Maimon, A. D. Straw, and M. H. Dickinson, "A simple vision-based algorithm for decision making in flying drosophila," *Current Biology*, vol. 18, no. 6, pp. 464–470, March 2008.
  - [40] M. Ballerini, N. Cabibbo, R. Candelier, A. Cavagna, E. Cisbani, I. Giardina, V. Lecomte, A. Orlandi, G. Parisi, A. Procaccini *et al.*, "Interaction ruling animal collective behavior depends on topological rather than metric distance: Evidence from a field study," *Proceedings of the National Academy of Sciences*, vol. 105, no. 4, p. 1232, 2008.
  - [41] Z. Wu, N. Hristov, T. Hedrick, T. Kunz, and M. Betke, "Tracking a large number of objects from multiple views," *IEEE International Conference on Computer Vision*, 2009.
  - [42] A. Straw, K. Branson, T. Neumann, and M. Dickinson, "Multi-camera real-time three-dimensional tracking of multiple flying animals," *Journal of The Royal Society Interface*, 2010.
  - [43] A. Elgammal, D. Harwood, and L. Davis, "Non-parametric model for background subtraction," *European Conference on Computer Vision*, pp. 751–767, 2000.
  - [44] K. Okuma, A. Taleghani, N. Freitas, J. Little, and D. Lowe, "A boosted particle filter: Multitarget detection and tracking," *European Conference on Computer Vision*, pp. 28–39, 2004.
  - [45] D. Zou, Q. Zhao, H. Wu, and Y. Chen, "Reconstructing 3d motion trajectories of particle swarms by global correspondence selection," in *IEEE International Conference on Computer Vision*. IEEE, 2009, pp. 1578–1585.
  - [46] S. GEMAN and D. GEMAN, "Stochastic relaxation, gibbs distributions, and the bayesian restoration of images," *IEEE Transactions on Pattern Analysis and Machine Intelligence*, vol. 6, no. 6, pp. 721–741, 1984.
  - [47] K. Murty, "An algorithm for ranking all the assignments in order of increasing cost," *Operations Research*, vol. 16, no. 3, pp. 682–687, 1968.
  - [48] M. Pascoal, M. Captivo, and J. Clímaco, "A note on a new variant of murty's ranking assignments algorithm," *4OR: A Quarterly Journal of Operations Research*, vol. 1, no. 3, pp. 243–255, 2003.
  - [49] C. Pedersen, L. Relund Nielsen, and K. Andersen, "An algorithm for ranking assignments using reoptimization," *Computers and Operations Research*, vol. 35, no. 11, pp. 3714–3726, 2008.
  - [50] R. Kohler, *Lords of the fly: Drosophila genetics and the experimental life*. University of Chicago Press, 1994.
  - [51] L. Vosshall, "Into the mind of a fly," *Nature*, vol. 450, no. 7167, pp. 193–197, 2007.
  - [52] E. comments comments comments comments, "No fruit fly an island?" *Nature methods*, vol. 6, no. 6, p. 395, 2009.
  - [53] L. Tammero and M. Dickinson, "The influence of visual landscape on the free flight behavior of the fruit fly *drosophila melanogaster*," *Journal of Experimental Biology*, vol. 205, no. 3, pp. 327–343, 2002.
  - [54] S. Fry, R. Sayaman, and M. Dickinson, "The aerodynamics of free-flight maneuvers in *drosophila*," *Science*, vol. 300, no. 5618, p. 495, 2003.